In silico and *in vitro* studies of potential inhibitors against Dengue viral protein NS5 Methyl Transferase from Ginseng and Notoginseng

Viwan Jarerattanachat [a], Chompunuch Boonarkart [b], Supa Hannongbua [c], Prasert Auewarakul [b], Ruchuta Ardkhean [d, *]

[a] NSTDA Supercomputer Center, National Electronics and Computer Technology Center, National Science and Technology Development Agency, Pathumthani, 12120, Thailand
[b] Department of Microbiology, Faculty of Medicine Siriraj Hospital, Mahidol University, Bangkok, Thailand
[c] Department of Chemistry, Faculty of Science, Kasetsart University, Bangkok, Thailand
[d] Princess Srisavangavadhana College of Medicine, Chulabhorn Royal Academy, Bangkok, 10210, Thailand

ABSTRACT

Background and aim: Dengue is a potentially deadly tropical infectious disease transmitted by mosquito vector *Aedes aegypti* with no antiviral drug available to date. Dengue NS5 protein is crucial for viral replication and is the most conserved among all four Dengue serotypes, making it an attractive drug target. Both Ginseng and Notoginseng extracts and isolates have been shown to be effective against various viral infections yet against Dengue Virus is understudied. We aim to identify potential inhibitors against Dengue NS5 Methyl transferase from small molecular compounds found in Ginseng and Notoginseng.

Experimental procedure: A molecular docking model of Dengue NS5 Methyl transferase (MTase) domain was tested with decoys and then used to screen 91 small molecular compounds found in Ginseng and Notoginseng followed by Molecular dynamics simulations and the per-residue free energy decompositions based on molecular mechanics/Poisson−Boltzmann (generalised Born) surface area (MM/PB(GB)SA) calculations of the hit. ADME predictions and drug-likeness analyses were discussed to evaluate the viability of the hit as a drug candidate. To confirm our findings, *in vitro* studies of antiviral activities against RNA and a E protein synthesis and cell toxicity were carried out.

Results and conclusion: The virtual screening resulted in Isoquercitrin as a single hit. Further analyses of the Isoquercitrin-MTase complex show that Isoquercitrin can reside within *both* of the NS5 Methyl Transferase active sites; the AdoMet binding site and the RNA capping site. The Isoquercitrin is safe for consumption and accessible on multikilogram scale. *In vitro* studies showed that Isoquercitrin can inhibit Dengue virus by reducing viral RNA and viral protein synthesis with low toxicity to cells ($CC_{50} > 20$ μM). Our work provides evidence that Isoquercitrin can serve as an inhibitor of Dengue NS5 protein at the Methyl Transferase domain, further supporting its role as an anti-DENV agent.

© 2022 Center for Food and Biomolecules, National Taiwan University. Production and hosting by Elsevier Taiwan LLC. This is an open access article under the CC BY-NC-ND license (http://creativecommons.org/licenses/by-nc-nd/4.0/).

1. Introduction

Dengue is a tropical infectious disease transmitted by the mosquito vector *Aedes aegypti.* It poses a significant threat to the health of the population in the tropical area where its vector resides. Dengue is endemic in more than 100 countries with millions of new cases of Dengue infection every year.[1] The area infested with the mosquito *Aedes aegypti* is likely to expand due to globalization and climate change, potentially posing even wider health risks.[2] The number of global Dengue infections is estimated to be half a million cases annually. This can lead to hospitalisation and life-threatening symptoms such as Dengue hemorrhagic fever (DHF) and Dengue shock syndrome (DSS).

Despite the adverse effects on the health and the local economy, Dengue remains a neglected disease with no specific antiviral drug

---

* Corresponding author.
E-mail address: ruchuta.ard@cra.ac.th (R. Ardkhean).
Peer review under responsibility of The Center for Food and Biomolecules, National Taiwan University.

Abbreviations

ADMET	absorption, distribution, metabolism, excretion, and toxicity
SAM	S-Adenosyl methionine
SAH	S-Adenosyl-L-homocysteine
SMILES	Simplified molecular-input line-entry system
MTase	Methyl Transferase
DENV	Dengue virus
MMFF	Merck Molecular Force Field
MD	Molecular Dynamics
NS	Nonstructural
3D	Three dimensional
RMSD	Root mean squared deviation
Da	Daltons
DHF	Dengue hemorrhagic fever
DSS	Dengue shock syndrome
ns	nanoseconds
RdRp	RNA-dependent RNA-polymerase
eg	*exempli gratia*
GTP	Guanosine 5′-Triphosphate
RVP	Ribavirin monophosphate

against it. Many antiviral compounds have entered clinical trials but have failed.[3] Dengue virus can be classified into four serotypes; DENV1, DENV2, DENV3 and DEN4, which are genetically related but antigenically distinct viruses. The challenges in drug development include compound efficacy against all four serotypes, toxicity and a brief therapeutic window. The only vaccine against Dengue, Sano-fi's Dengvaxia®, has contraindicated effects in children and induced more severe symptoms in subsequent infections in individuals that have never been infected by Dengue before the vaccination.[4] Therefore, finding antiviral agents that are effective against the virus can be considered as an urgent medical need.

Dengue virus (DENV) belongs to genus *Flavivirus,* the family of *Flaviviridae.* Other disease-causing *Flaviviruses* transmitted by mosquito vector *Aedes aegypti* includes Zika, West Nile, yellow fever virus and Japanese encephalitis virus.[5] DENV has a positive-sense viral RNA genome encodes for structural and non-structural proteins; structural C, E, prM and non-structural: NS1, NS2A, NS2B, NS3, NS4A, NS4B, and NS5. The largest is NS5 protein which is essential for viral RNA replication. The NS5 protein consists of two enzymatic sites or domains; an RNA-dependent RNA-polymerase (RdRp) near the N terminal region and Methyl transferase (MTase) near the C terminal region.[6,7] The MTase domain consists of two active sites, the RNA capping site (Guanosine 5′-Triphosphate (GTP) binding pocket) in proximity with the AdoMet binding site. The native ligand at the AdoMet binding site is a small molecule methylating agent, S-Adenosyl methionine (SAM or AdoMet). SAM can deliver a methyl group to the ribonucleotide of the capped viral RNA chain residing at the RNA capping site. After methylation, SAM is converted to S-Adenosyl-L-homocysteine (SAH or AdoHcy) upon the loss of the methyl group.

NS5 protein is the most conserved protein in all four Dengue serotypes and is highly conserved in all Flaviviruses, making it a promising target for broad-spectrum antiviral drug development.[8] One of the challenges of targeting MTases is the selectivity of inhibiting viral MTase over human MTase.[9,10] Due to the interest in NS5 MTase as a drug target, many groups have experimentally or virtually screened various compound datasets against the enzyme. Some examples of compound databases explored are cyclic pep-tides, flavones derivatives, IBS natural compound library,

adamantane derivatives, NCI diversity set II library, small-fragments database and a large database of over 5 million commercially available compounds.[10,11]

1.1. Ginseng and Notoginseng

Ginseng is one of the most popular herbs that has been tradi-tionally used in many parts of the world such as Korea, China, and Siberia as far back as thousands of years ago.[12] The highly-prized Panax Ginseng (Meyer, Korean Ginseng, Red Ginseng) and its less well-known relative, Panax Notoginseng (Burkill, Sanchi Ginseng) are two of over ten species belong to the Panax genus, Araliaceae family.

The health benefits of Ginseng and Notoginseng are diverse. Ginseng extracts and isolates have shown antiviral, anti-microbial, anti-inflammatory, anti-ageing and immuno-modulatory activities. They are used for the treatment and prevention of cardiovascular disease, neurological disorders, cancer and diabetes.[13–16] Ginseng was reported as a promising adjuvant for the treatment of viral diseases such as SARS-CoV-2.[17,18] Regarding their antiviral activ-ities, Ginseng can inhibit, or show protective effects against a range of viruses such as Hepatitis B, Human Rotavirus, H5N1 influenza virus, H1N1 influenza A virus and respiratory syncytial virus (RSV).[17] A formula containing both Ginseng and Notoginseng has been used in the recovery phase for DENV-infected patients in China.[19] Only recently, in early 2022, Notoginseng isolates were found to show anti-Dengue activity in Zebrafish.[20] A recent report in 2021 on medicinal plants against Dengue virus has not high-lighted Ginseng or Notoginseng as potential herbs against the vi-rus.[21] With the antiviral activities and a wide range of health benefits of Ginseng and Notoginseng extracts and isolates, we explore the potential of chemicals found in Panax Ginseng and/or Panax Notoginseng as antiviral agents against Dengue NS5 Methyl transferase (MTase).

1.2. Virtual screening by molecular docking

Molecular docking is one of the popular methods used for structure-based virtual screening.[22] The docking scores reflect favorable predicted poses of ligands which can vary depending on the algorithms used.[23] A study by Shoichet, Roth and Irwin utilised molecular docking as a tool to screen an ultra-large library. Their models, supported by experimental verifications, significantly enriched real positives when the docking scores exceeded a threshold.[24,25] Many *in silico* studies performed docking and MD studies in tandem to identify potential inhibitors.[26–28] Molecular Dynamics (MD) simulation is a time-dependent technique which can capture protein dynamics and has been widely used to predict relative binding affinities of a ligand bound to a target protein.[29] In this work, we used these methods to investigate chemicals found in Panax Ginseng and/or Panax Notoginseng as potential inhibitors against DENV NS5 MTase. To analyse the viability of the hit com-pounds as drug candidates, chemical absorption, distribution, metabolism, excretion, and toxicity (ADMET), drug-likeness and compound accessibility are discussed.

2. Materials and methods

2.1. Molecular docking

Open access software; Ledock and Autodock vina 1.1.2 were used for molecular docking.[30,31] X-ray crystal structures of DENV3 and DENV2 NS5 methyl transferases (PDB ID: 4r8s, 5e9q and 1r6a) were retrieved from RCSB PDB protein data bank (https://www.rcsb.org). The protein structures are aligned using PyMOL.[32] All solvents,

metals and counter ions are removed. The 3D structures of the ligands are extracted from protein complexes and are used as reference biological poses during model validations. Protein structures are prepared according to the protocols of each software (see Supporting Information). Using Autodock Tools 1.5, the grid box is defined around the AdoMet binding site as a cuboid space of size 20 × 20 × 20 Å^3 centred at the location where the native ligands, SAM and SAH reside. Decoys, in SMILES format, are generated from the Database of Useful Decoys: Enhanced or DUD-E (http://dude.docking.org) based on the SMILES molecular representation of SAM as obtained from the RCSB PDB protein data bank. The 3D structures of 44 decoys are generated from the SMILES representations using Open Babel with the MMFF94 force field.[33,34] Protonation states of ligands are generated with Open Babel or open access scripts prepared at pH 7.4.[35] For virtual screening, protein preparation was done with LePro (PDB ID 4r8s) and molecular docking was carried out with LeDock with clustering RMSD of 0.5 Å, producing 25 poses for each screening entry.[31] The 3D structures of 91 compounds found in Ginseng and Notoginseng were acquired from the literature and PubChem database (https://pubchem.ncbi.nlm.nih.gov) including their protonated forms (where applicable), giving total of 94 structures. The root mean squared deviation (RMSD) of heavy atoms in the docked poses compared to the biologically active conformations (reference poses) were calculated using Obrms tool in Open Babel.[33,34] The visualisation was done by Maestro and PyMOL.[32,36]

2.2. ADMET calculations

ADME predictions were calculated from SWISSADME server (http://www.swissadme.ch) from SMILES strings obtained from PubChem database.[37] The hERG-related toxicity prediction was calculated using CardPred server (http://ssbio.cau.ac.kr/CardPred).

2.3. Molecular dynamics simulations

The molecular dynamics (MD) simulations were performed using GROMACS 2020[38] with the AMBER ff14SB forcefield[39] for protein, General Amber Force Field (GAFF2)[40] for ligands and TIP3P water models.[41] The system coordinates and topologies were prepared using AmberTool21, and converted to use in GROMACS *via* ParmEd.[42,43] The ligand geometry optimisation and partial charge calculation were performed using Gaussian16 at HF/6-31G* level of theory.[44] The ligand topology was generated using Antechamber with RESP model.[45] For the AdoMet binding site, the complex system was prepared using tleap where the Isoquercitrin-NS5 docked complex was used as an initial structure. Protonation states and histidine tautomers were also kept similar to the docked structure. The system was solvated by TIP3P water molecules with a 10 Å buffering distance. Counterions were added to neutralise the system. For the RNA capping site, the snapshots at 480 ns, 490 ns, and 500 ns of AdoMet#3 were used as initial systems for RNA#1, RNA#2, and RNA#3, respectively. The simulated system was subjected to energy minimization and preformed for 500 ns with 2 fs integration time step for the production run. The temperature was set to 310 K using v-rescale algorithm,[46] the isotropic pressure was set to 1 bar using Parrinello-Rahman algorithm.[47] The LINCS constraints were applied to all bonds with hydrogen atoms.[48] The long range electrostatic was calculated using particle-mesh Ewald (PME) with 0.12 nm grid spacing.[49] The Verlet cut-off scheme with 1.2 nm cut-off distance was applied for short-range Coulomb and van der Waals interactions. The simulations were repeats with different random velocities. Periodic boundary condition was applied in all directions. The analysis processes were perform using GROMACS utilities. The per-residue free energy decomposition based on

molecular mechanics/Poisson−Boltzmann (generalised Born) surface area (MM/PB(GB)SA) method was calculated by using gmx_MMPBSA version 1.52 based on MMPBSA.py version 16.0 using 100 snapshots from the last 10 ns.[50,51] Trajectories were subject to be least square fitted in both translation and rotation before performing the energy calculation. The visualisation was done by VMD and PyMOL.[32,52]

2.4. In vitro viral inhibition testing

Vero cells (African green monkey kidney) were cultured in Minimum Essential Medium (MEM; Corning) supplemented with 10% heat-inactivated fetal bovine serum (FBS; Gibco) at 37 °C with 5% CO_2. *Aedesalbopictusmosquito* cells (C6/36) were maintained at 28 °C in Leibovitz 15 supplemented with L-glutamine and 10% heat-inactivated FBS.

Dengue 2 virus (DENV 2) strain 16681 were propagated in C6/36 cells. Virus titers were determined by measuring focus-forming units in Vero cells.

Isoquercitrin (Sigma-Aldrich) was evaluated the cytotoxicity in Vero cells by 3-(4,5-Dimethylthiazol-2-yl)-2,5-Diphenyltetrazolium Bromide (MTT) dyes (Invitrogen). Monolayer Vero cells were infected at multiplicity of infection (MOI) 0.2 of DENV 2 for 2 h. After viral inoculation, the viruses were discarded. The cells were washed with MEM and the media containing Isoquercitin at various concentration or 0.5% Dimethyl sulfoxide (DMSO, control) were added. The cells were further incubated at 37 °C, 5% CO_2 for 2 days. After the incubation time, cells were collected for the viral RNA and E protein quantification.

Total RNA was extracted using Trizol reagent (Invitrogen). The concentration of DENV2 RNA was determined by real-time reverse transcription PCR (qRT-PCR). The primer pairs were provided as follows; pan dengue forward (5′TTGAGTAAACYRTGCTGCCTG TAGCTC3′) and pan dengue reverse (5′ GAGACAGCAGGATCTCTGGT CTYTC3′); GAPDH forward (E14134: 5′CAACTACATGGTTTAC ATGTTC3′) and GAPDH reverse (E14135: 5′GCCAGTGGACT CCACGAC3′).[53,54] The qRT-PCR was performed using the Sensi-FAST™ SYBR® No-ROX One-Step Kit (Meridian Bioscience) in LightCycler® 480 (Roche). RNA extracted from DENV2-infected cell was serially diluted and used for standard curve setting.

The DENV2 protein were determined with 4G2 as primary antibody for a detection of the viral E protein. Cells were fixed with ice-cold acetone:methanol (1:1) for 20 min. Primary antibody was added and incubated for 1 h at 37 °C. Then the cells were washed with 0.05% Tween® detergent in phosphate buffer saline (PBS), incubated in secondary antibody, horseradish peroxidase (HRP)-conjugated anti-mouse goat antibody (Dako), for 1 h in 37 °C. After incubation, the cells washed with 0.05% Tween® detergent in PBS. Next, the tetramethylbenzidine (TMB) peroxidase substrate system (KPL, USA) was added and incubated at room temperature in the dark for 10 min. Finally, the reaction was stopped with 1 M sulfuric acid. The optical density (OD) was measured at 450/630 nm at room temperature.

The percentage of DENV inhibition were normalized to the solvent control (0.5% DMSO), and the half maximal inhibitory concentration (IC_{50}) was calculated by non-linear regression analysis of the dose-dependent response graph using GraphPad Prism version 8.[55]

3. Results and discussions

3.1. Molecular docking model validation and cut-off determination

Competitive inhibition is when an inhibitor competes with the enzyme's substrate or co-factor for the same binding site.

Competitive inhibition of NS5 MTase by small molecule non-covalent inhibitors have been unequivocally proven by X-ray crystallography at both of its active sites namely, Sinefungin (SFG) in the AdoMet binding site and Ribavirin monophosphate (RVP) in the RNA capping site.[56,57] To discover small molecules that can potentially bind to the MTase active sites, we first examine the AdoMet binding site by molecular docking. We anticipated that if we attempt to find a competitive inhibitor at the AdoMet binding site, we will have a higher chance of success compared to the RNA capping site (GTP binding site) because the co-factor, SAM, is a small molecule as opposed to a polymeric RNA chain.

To validate our models, we examined if the models can reproduce the biologically active poses of the ligands by redocking (putting back the ligand) and cross-docking (putting back ligands that belongs to different ligand-protein complex). For reference data, we collated structures of five NS5 MTase complexes with ligands at the AdoMet binding site from a public structural depositry (https://www.rcsb.org) PDB ID: 5E9Q, 1R6A, 4R8S, 3P8Z and 5ULP.

The overlaid X-ray crystallographic structures of selected ligand-NS5 MTase complexes are shown in Fig. 1, with five ligands residing in the AdoMet binding site and RVP residing in the RNA capping site. Four of five ligands bound at AdoMet site (SAM, SAH, SFG and 36A) are from DENV NS5 MTase complexes, while one of them is an inhibitor of the closely related NS5 MTase of Zika virus (KB1).

Our first criterion for a suitable molecular docking model is the model predicted the top pose (pose with the lowest docking score) that resembles the reference pose (X-ray crystal structure) with small root mean square deviations (RMSD) within an acceptable range of 2 Å.[23] Multiple docking models generated with Autodock Vina and LeDock predicted top-scoring poses with RMSD lower than 2 Å (see the Supporting Information).[30,31] To select the best-performing models, we carried out molecular docking of these ligands with the decoys.

3.1.1. Docking of active ligands and decoys

We hypothesised that a model that can separate real ligands from decoys will be more likely to produce enriched real hits during virtual screening, given that the docking scores fall within the region of active ligands. Decoys are compounds with similar chemical properties to the ligand but with different structures as defined by Irwin and Shoichet.[58] We generated decoys based on SMILES representation of SAM from the Database of Useful Decoys: Enhanced (DUD-E) web server (http://dude.docking.org).

To select the docking models, we used two criteria: 1) Docking scores of all active ligands form a cluster, rather randomly or evenly spread out among a wide range of scores, and 2) the compound with the lowest docking score is an active ligand, rather than a

decoy. A model created from DENV 3 (PDB ID 4r8s) with LeDock passed the criteria. The docking scores from 5 ligands (blue) and 44 decoys (grey) are shown in Fig. 2.

The predicted docking scores of the ligands lie between −10.9 and −9.3 kcal/mol. The scores of the decoys range between −6.1 and −9.8 kcal/mol. Out of 44 decoys, the docking scores of four of the top-scoring decoys are in the range of active ligands. According to these results, we set a threshold for virtual screening of compounds at around −9.0 kcal/mol. Thus, this molecular docking protocol was used in the next step for virtual screening of herbal compounds. During the virtual screening, compounds whose docking scores are lower than or equal to this threshold will be considered as 'hits'. However, compounds that do not pass the threshold does not necessarily mean that they have no potential to bind to the enzyme. In this work, we further investigate only the 'hits' in the subsequent studies.

3.2. Screening of herbal compounds

Over 200 compounds were found in Ginseng and over 100 in Notoginseng. Ginseng and Notoginseng have many compounds in common. These include ginsenosides, phytosterols, sesquiterpenes, flavonoids, polyacetylenes, alkaloids and phenolic compounds.[59–61]

In this study, only compounds whose 3D structures have been elucidated are included. This filters off compounds that lack information about most of their stereochemistry which is likely to be important in molecular recognition. Only compounds with molecular weights of less than 500 Da were retained. Larger molecules with molecular weights greater than 500 Da are excluded because the AdoMet binding site is a highly conserved region that is well-
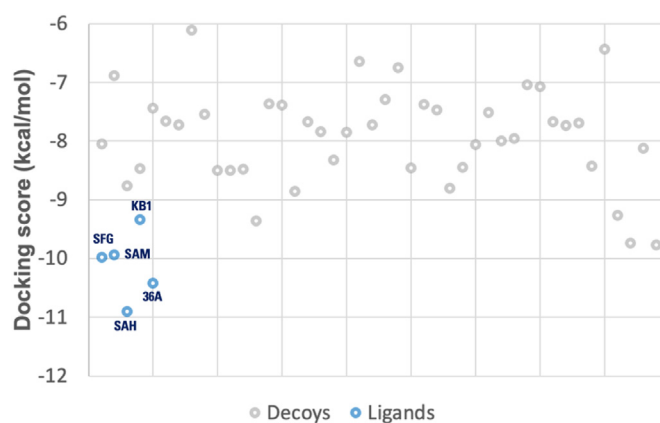

Fig. 2. Docking scores of the five ligands and the decoys against the DENV NS5 MTase.
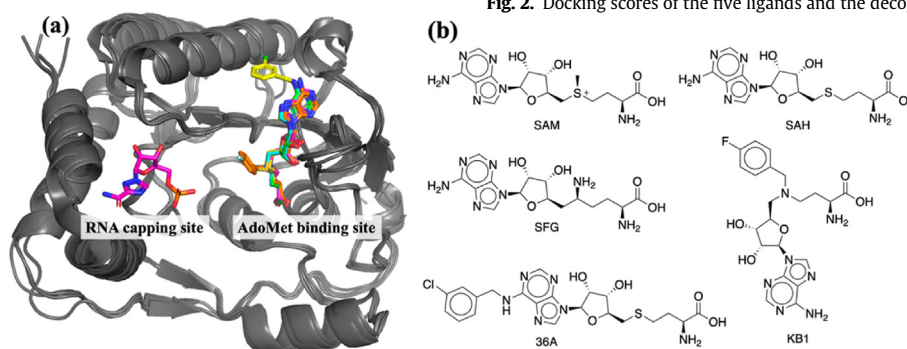

Fig. 1. a) Superimposed 3D structures of NS5 MTase with ligands at AdoMet binding site (PDB ID: 5E9Q (SAM, cyan), 1R6A (SAH, pink), 4R8S (SFG, green), 3P8Z (36A, yellow), 5ULP (kb1, orange) and RVP (pink) at RNA capping site, b) Structures of AdoMet binding site ligands used as references in this study.

buried and has evolved to accommodate SAM and SAH (399 DA and 384 Da respectively). Larger and heavier molecules are less likely to fit in the pocket and do not comply with drug-likeness criteria eg. Lipinski's rule of five. Saturated hydrocarbons or unsaturated hydrocarbons with only one multiple bond are excluded because these compounds are not likely to form fruitful molecular interactions. As a result, we collected a database of 91 compounds for virtual screening against DENV NS5 MTase. Using the validated molecular docking model, the docking scores of the top 20 compounds screened are tabulated in Table 1. The docking scores for the rest of the compounds screened can be found in Supporting Information.

Out of the 91 small molecules screened, we found that Isoquercitrin is the only compound that passed the preset cut-off threshold with the docking score of −9.0 kcal/mol. The interactions between the top-scoring docked pose of Isoquercitrin and MTase is shown in Fig. 3.

The top-scoring pose of Isoquercitrin forms hydrogen bonds with protein residues Cys82, Gly86, Trp87 Asp146 and Lys180 with bond lengths range from 1.7 to 2.2 Å. Hydrogen bonds between Isoquercitrin and Lys180 and Trp87 falls within the range of strong hydrogen bonds with high covalent character (2.2–2.5 Å).[62] However, other hydrogen bonds are clearly shorter than the optimal range. This prompt us to further examine the binding of Isoquercitrin to MTase with molecular dynamics simulations.

3.3. Molecular dynamics simulations

To further examine the binding of Isoquercitrin and the stability of the Isoquercitrin-MTase complex, the complex was relaxed and equilibrated, followed by a production run for 500 ns. The MD simulations were carried out in triplicates in two parts. In the first part, the structure of Isoquercitrin obtained from molecular docking at AdoMet binding site was optimised with DFT calculations prior to MD simulations (AdoMet#1, AdoMet#2 and AdoMet#3). In the second part, a snapshot at end of the 500 ns simulation of the third repeat (AdoMet#3) where Isoquercitrin had moved to the RNA capping site was further simulated for another 500 ns (RNA#1, RNA#2, and RNA#3).

The analysis of C_α RMSD showed that the whole complex was stable with C_α RMSD of less than 2 Å throughout the 500 ns simulations in all six simulations (Fig. 4a and b).

To examine the fluctuations in each individual protein residue of the ligand-bound complex, the root mean square fluctuations (RMSF) of C_α for each residue were analysed (Fig. 4c and d). The RMSF is relatively larger at the terminal residues (highlighted with a pink surface, Fig. 4e). This is expected for typical MD simulations because the terminal residues can move with fewer restrictions. The X-ray structure of MTase (PDB ID: 4r8s), superimposed with the simulated structure snapshots at 500 ns visually showed little fluctuation at the active sites Fig. 4e; the simulated protein structures where Isoquercitrin reside at the AdoMet binding site (blue mesh) are shown in light blue ribbons (AdoMet#1—2), whereas the protein structures where Isoquercitrin reside at the RNA capping site (white mesh) are shown in yellow ribbons (AdoMet#3 and RNA#1—3). In all six simulations, the residues 40—47 and residues 106—109 showed higher RMSF (highlighted with a pink surface) and were similar in both parts of the simulations even when the ligand resided at different sites. This suggests that MTase remained relatively stable with insignificant conformational changes upon binding of Isoquercitrin.

To examine the behaviour of Isoquercitrin in the Isoquercitrin -MTase complex, the RMSD of Isoquercitrin and the 3D structures of Isoquercitrin in the binding sites of the simulated complexes were analysed and shown in Fig. 5. When started with the ligand at the AdoMet binding site, two out of three simulations showed that Isoquercitrin had shifted within 5 Å in the same site (AdoMet#1—2 in black and red respectively, Fig. 5a). The RMSDs of Isoquercitrin indicated that the binding was relatively stable for the duration of the simulations. Interestingly, the RMSD of Isoquercitrin in the third simulation (AdoMet#3 in green) showed that Isoquercitrin had moved from the AdoMet binding site to the GTP binding site (RNA capping site) and had remained there for at least 200 ns towards the end of the simulation.

To visualise the overall movements of Isoquercitrin, the starting pose (relaxed docked pose) and each snapshot at 500 ns from the triplicate runs are shown in Fig. 5b; the first simulation (AdoMet#1, carbons shown in cyan), the second simulation (AdoMet#2, carbons shown in green) and the third simulation (AdoMet#3, carbons shown in yellow). The starting docked pose (relaxed) is shown in light grey for comparison. The results from the first two simulations showed that the ligand shifted slightly deeper into the binding pocket and was relatively stable throughout the simulations (Fig. 5b). In the third simulation (AdoMet#3, carbons shown in

Table 1
Docking scores and molecular weights of the top 20 compounds found in Ginseng and/or Notoginseng, ranked by their docking score against the DENV NS5 Methyl Transferase.

| Compound names	Molecular Weight (Da)	DENV MTase (kcal/mol)
Isoquercitrin	464.4	−9.0
Quercetin	302.2	−7.7
Adenosine	267.2	−7.4
Syringin	372.4	−7.3
p-Glucosyloxymandelonitrile	311.3	−7.2
Pancratistatin	325.3	−7.1
Dianthramine	289.2	−7.0
Protopanaxatriol	476.7	−6.9
Kaempferol	286.2	−6.8
Gypenoside-A	336.4	−6.7
Ramalic acid	346.3	−6.6
Suchilactone	368.4	−6.3
Celabenzine (H⁺)	380.5	−6.3
Protopanaxadiol	460.7	−6.3
Dencichin (H⁺)	177.1	−6.3
5-(E)-heptadec-12-enyl benzene-1,3-diol	346.5	−6.3
(3R,8E,10S)-10-hydroperoxyheptadeca-1,8-dien-4,6-diyn-3-ol	276.4	−6.2
(3S,5R,8R,9R,10R,14R,17S)-17-(2-hydroxy-6-methylhept-5-en-2-yl)-4,4,8,10,14-pentamethyl-2,3,5,6,7,9,11,12,13,15,16,17-dodecahydro-1H-cyclopenta[a]phenanthren-3-ol	444.7	−6.2
Ginsenoyne B	294.8	−6.2
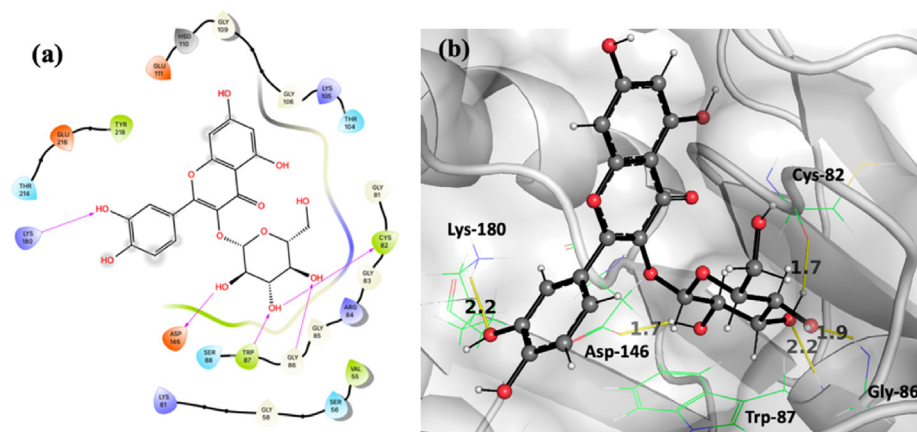
Fig. 3. Top-scoring pose of Isoquercitrin in AdoMet binding site, overlaid with the protein DENV NS5 MTase (PDB ID:4r8s) a) Hydrogen bond interactions (purple arrows) in 2D representation, b) Hydrogen bonds (yellow lines) lengths (Å) in 3D representation.

yellow), Isoquercitrin had moved and resided in the RNA capping site by the end of the simulation.

We took a snapshot at the end of this simulation and carried out molecular dynamics simulations for another 500 ns in triplicates (RNA#1−3). The RMSDs of Isoquercitrin were approximately 2.5 Å from the starting position, indicating that the binding of the ligand at the RNA capping site was relatively stable in all three simulations (RNA#1−3 in blue, pink and orange respectively, Fig. 5c). The superimposed 3D structures of the Isoquercitrin-MTase complex from the snapshots at 500 ns of the triplicates are shown in Fig. 5d; the first simulation (RNA#1, carbons shown in yellow), the second simulation (RNA#2, carbons shown in purple), and the third simulation (RNA#3, carbons shown in grey). The starting pose is shown in white for comparison (AdoMet#3 in Fig. 5d).

The results demonstrate that Isoquercitrin can bind to the NS5 MTase and reside at the AdoMet binding site and has the potential to also bind at the RNA capping site. Notably, recent *in silico* studies done by Kumaradhas and co-workers have demonstrated that four flavonoid molecules, including Quercetin, are potential inhibitors of NS5 MTase at the RNA capping site, in agreement with behavior of Isoquercitrin observed in our work.[63]

To analyse the interactions between Isoquercitrin and the protein residues, per-residue free energy decompositions based on molecular mechanics/Poisson−Boltzmann (generalised Born) surface area (MM/PB(GB)SA) method are tabulated with a cut-off at ± 1 kcal/mol (Table 2, at AdoMet binding site and Table 3 at RNA capping site).

The interactions between Isoquercitrin with the protein residues at the AdoMet binding site showed significant free energy contributions upon binding with residues Gly81, Gly83, Thr104, Lys105, Gly109, His110, Glu111, Asp131 Asp146 and Ile147. The majority of these residues are in agreement with previous experimental work done by others; Canard and coworkers examined crystal structures of Dengue MTase and SAH molecule. They found that SAH was stabilized by hydrogen bonds with Lys105 and Asp131 residues, and SAH was located in a hydrophobic pocket made up of Thr104, Lys105 and Ile147 residues.[7] Luo and co-workers showed that Glu111 is a key residue for viral replication.[64] Dong and co-workers showed that mutations of residues His110 with alanine affected methylation activities.[65]

The interactions between Isoquercitrin with the protein residues at the RNA capping site showed significant free energy contributions upon binding with residues Lys14, Asn18, Arg22, Phe25, Lys29, Glu149, Ser150, Ser151, Pro152 and Ser213. Canard and coworkers reported that conserved residues, Lys14 and Asn18 form

hydrogen bonds to ribonucleotides and the phenyl ring of Phe25 can stack with a purine of ribonucleotides in crystal structures.[7] They also observed that K29Q mutation destroyed the ability of MTase to bind with GTP. Mutations at N18A or S150A significantly reduced GTP binding.

3.4. In vitro viral inhibition testing

For the antiviral activity testing, cytotoxicity of Isoquercitrin was first determined in Vero cell using the MTT assay. The 50% cytotoxic concentration (CC_{50}) of this compound is greater than 20 μM. To study the effect of Isoquercitrin on Dengue RdRp inhibition and protein synthesis, dengue infected cells were treated with Isoquercitrin and the concentration of viral RNA and a representative viral E protein were measured. Isoquercitrin showed inhibitory activity against the viral RNA synthesis with an IC_{50} of 6.5 μM (Fig. 6), in accordance with previous published data.[66] Interestingly, the viral protein synthesis was inhibited at a significantly lower IC_{50} of 2.5 μM ($p < 0.05$, unpaired t-test). At this concentration the inhibition of viral RNA synthesis was negligible.

Therefore, the inhibitory activity of the viral protein synthesis at this concentration with unperturbed level of viral RNA could not be caused by viral RNA synthesis inhibition. This indicated that in addition to RdRp inhibition, Isoquercitrin also inhibited the viral protein translation. The finding supports the inhibitory activity of Isoquercitrin against Dengue NS5 MTase, which is required for the viral mRNA capping and translation.[7]

3.5. Evaluation of Isoquercitrin as a viable antiviral agent: ADMET properties, drug-likeness and accessibility

Isoquercitrin, also known as Isotrifolin, Hirsutrin or Quercetin-3-O-glucoside is found in *Panax Ginseng* as well as many other herbs such as Ginkgo (*Ginkgo biloba*) and Neem (*Azadirachta indica*), some fruits and vegetables such as onions (*Allium cepa*) and Indian gooseberries (*Phyllanthus emblica*).[67] Isoquercitrin is a glycoside form of a flavone, Quercetin, with a furanose ring which can be converted to a pyranose form called Isoquercetin. Therefore the two forms are considered to have identical biological functions.[68] Isoquercitrin is accessible on a multikilogram scale *via* an enzymatic reaction.[69]

Isoquercetin has been referred to as a broad-spectrum antiviral.[70] It was shown to inhibit Zika virus, Ebolavirus, Herpes Simplex virus, Varicella-Zoster virus and Human Cytomegalovirus.[70] Relating to Dengue virus, Isoquercitrin has been found to reduce
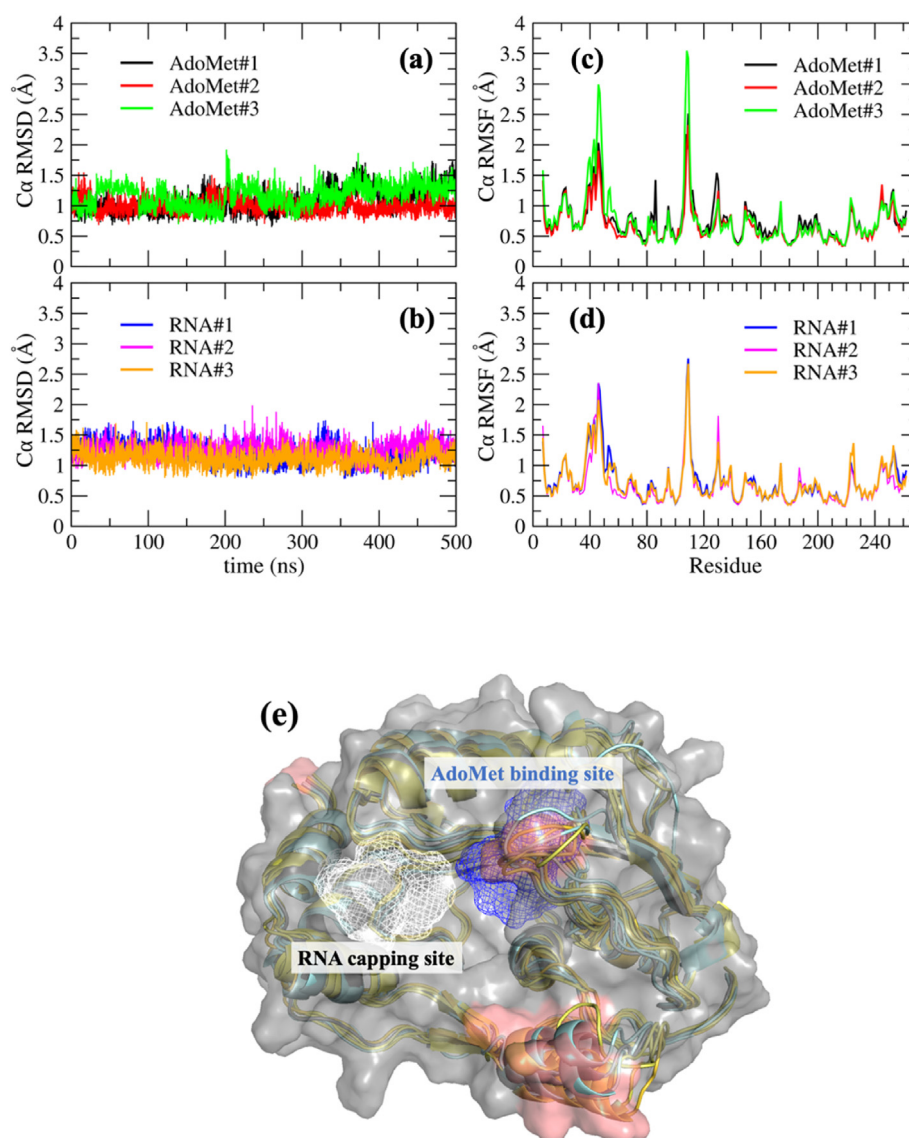
Fig. 4. a) RMSD of the complex's C_α (Å) over 500 ns starting with ligand at AdoMet binding site (shown as blue mesh in 4e) in three replicates: AdoMet#1 (black), AdoMet#2 (red) and AdoMet#3 (green), b) RMSD of the complex's C_α (Å) over 500 ns starting with ligand at RNA capping site (shown as white mesh in 4e) in three replicates: RNA#1 (blue), RNA#2 (pink) and RNA#3 (orange), c) RMSF of the residue's C_α (Å) starting with ligand at AdoMet binding site in three replicates: AdoMet#1 (black), AdoMet#2 (red) and AdoMet#3 (green), d) RMSF of the residue's C_α (Å) starting with ligand at RNA capping site in three replicates: RNA#1 (blue), RNA#2 (pink) and RNA#3 (orange) and e) X-ray structure of MTase (grey ribbon, PDB ID: 4r8s) superimposed with snapshots at 500 ns of all six MD simulations (AdoMet#1–2 in cyan ribbons, AdoMet#3 and RNA#1–3 in yellow ribbons). High RMSF regions are represented in pink surfaces.

in vitro activity of DENV NS2B-NS3 protease with IC$_{50}$ of 42–44 μM and inhibited NS5 RdRp activity with IC$_{50}$ of 9.5 μM.[66,71]

Many studies have shown that Isoquercitrin is safe for consumption.[72,73] As an adjuvant, Isoquercitrin has been tested for its safety in clinical trial phase II.[74] Compared to quercitrin, Isoquercitrin has better oral bioavailability.[75] Following ingestion, Isoquercitrin is rapidly metabolized while after an intravenous injection, the molecule can be detected in rat urine at 24 h. ADMET properties and drug-likeness predictions of Isoquercitrin are included in the Supporting Information. The safety profile, bioavailability and accessibility of Isoquercitrin make it a promising candidate to be further investigated as a viable drug.

4. Conclusion

Virtual screening of 91 compounds found in Ginseng and Notoginseng against the DENV NS5 MTase domain yielded Isoquercitrin as a single hit. Molecular dynamics simulations and per-residue free energy decompositions based on (MM/PB(GB)SA) suggested that Isoquercitrin formed a relatively stable complex with DENV NS5 MTase and demonstrated the potential to bind to the protein at both of its active sites: AdoMet binding site and RNA capping site. The interactions with key residues are in agreement with previous experimental studies. In terms of the viability of Isoquercitrin as a drug candidate, Isoquercitrin is accessible in a large scale and many studies and clinical trials have indicated that Isoquercitrin is safe for consumption. *In vitro* viral inhibition study showed that Isoquercitrin can inhibit Dengue viral RNA synthesis at an IC$_{50}$ comparable to previous data on RdRp inhibition. It also showed higher inhibitory activity on the viral protein synthesis with a significantly lower IC$_{50}$. This supports the inhibition of Isoquercitrin against the NS5 MTase. The double action of Isoquercitrin
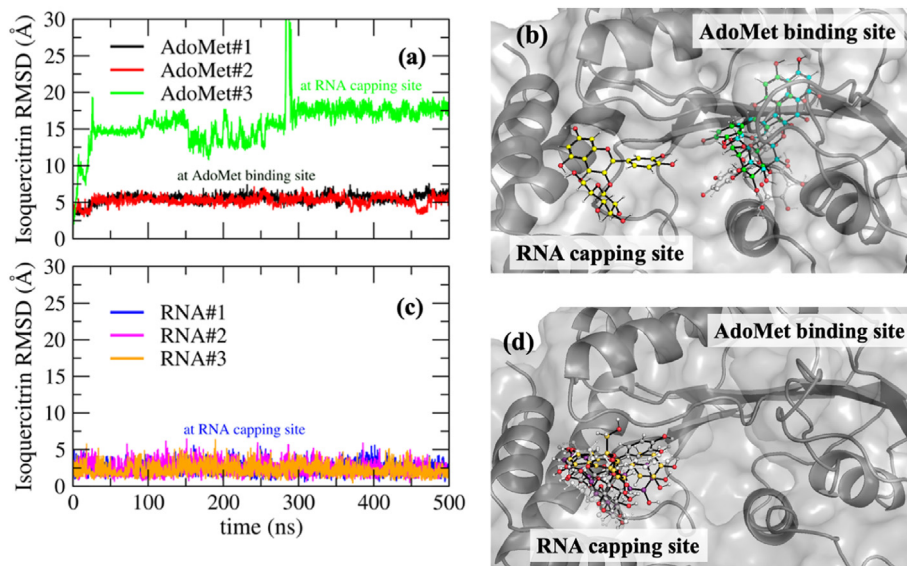
Fig. 5. a) RMSD of Isoquercitrin (Å) over 500 ns, starting with ligand at AdoMet binding site, in three replicates: first (AdoMet#1 in black), second (AdoMet#2 in red) and third (AdoMet#3 in green), b) Superimposed structures of Isoquercitrin showing the AdoMet binding site and the RNA capping site: staring from docked pose (relaxed) in light grey and after 500 ns simulations in three replicates: first (AdoMet#1 in cyan), second (AdoMet#2 in green) and third (AdoMet#3 in yellow) c) RMSD of Isoquercitrin (Å) over 500 ns, starting with ligand at RNA capping site, in three replicates: first (RNA#1 in blue), second (RNA#2 in pink) and third (RNA#3 in orange), and d) Superimposed structures of Isoquercitrin showing the AdoMet binding site and the RNA capping site: a starting pose (snapshot at 500 ns of AdoMet#3) shown in white and snapshots after 500 ns simulations of the three replicates: first (RNA#1 in yellow), second (RNA#2 in purle) and third (RNA#3 in grey).

Table 2
Per-residue free energy decompositions (MM/PBSA and MM/GBSA) at AdoMet binding site.

Residues	MM/GBSA (kcal/mol)		MM/PBSA (kcal/mol)	
	AdoMet#1	AdoMet#2	AdoMet#1	AdoMet#2
Gly81	−1.10 ± 0.37	−1.08 ± 0.40	0.90 ± 0.37	0.19 ± 0.40
Gly83	−1.70 ± 0.39	−0.49 ± 0.5	−1.37 ± 0.39	−0.29 ± 0.50
Thr104	−1.58 ± 0.75	−1.26 ± 0.71	−0.84 ± 0.76	0.19 ± 0.70
Lys105	−0.97 ± 1.28	−0.80 ± 1.34	−1.16 ± 1.26	−0.43 ± 1.34
Gly109	−1.14 ± 0.39	0.08 ± 0.43	−0.32 ± 0.38	0.19 ± 0.43
His110	−3.74 ± 0.59	−0.65 ± 0.78	−3.50 ± 0.59	0.78 ± 0.79
Glu111	−8.06 ± 1.21	−3.07 ± 1.96	−6.71 ± 1.21	−1.40 ± 1.93
Asp131	−1.76 ± 1.04	−2.35 ± 1.43	−0.40 ± 1.06	−1.85 ± 1.46
Asp146	−6.44 ± 1.74	−2.97 ± 2.24	−5.10 ± 1.73	−2.24 ± 2.27
Ile147	−2.15 ± 0.57	−2.07 ± 0.48	−1.87 ± 0.57	−1.55 ± 0.49

Note: ± represents the standard errors of the mean.

on both RdRp and MTase makes it an attractive antiviral compound. Our work provides findings which can contribute to the development of Isoquercitrin as an anti-DENV agent.
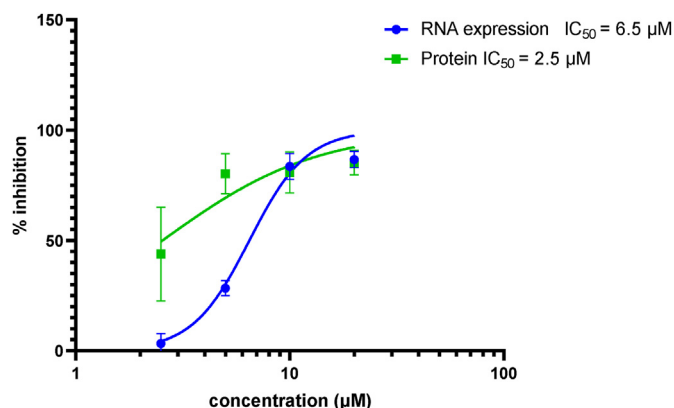

Fig. 6. Antiviral activity of isoquercitrin against DENV2 *in vitro*. Vero cells were infected with DENV 2 at MOI 0.2, and then treated with 20, 10, 5 and 2.5 μM of isoquercitrin or with 0.5%DMSO (virus control). At 48h post infection cells were determine the RNA expression level and protein level of DENV2 virus. The experiments were performed independently in triplicate. Error bar showed mean ± SD.

Table 3
Per-residue free energy decompositions (MM/PBSA and MM/GBSA) a RNA capping site.

Residues	MM/GBSA (kcal/mol)				MM/PBSA (kcal/mol)			
	AdoMet3	RNA1	RNA2	RNA3	AdoMet3	RNA1	RNA2	RNA3
Lys14	0.26 ± 0.97	0.08 ± 1.05	0.02 ± 1.07	0.22 ± 1.12	2.14 ± 0.95	1.99 ± 1.02	1.21 ± 1.00	1.77 ± 1.14
Asn18	−2.85 ± 0.64	−2.83 ± 0.63	−3.00 ± 0.58	−2.94 ± 0.56	−3.23 ± 0.64	−3.21 ± 0.63	−3.48 ± 0.58	−3.41 ± 0.56
Arg22	−0.69 ± 1.48	−0.59 ± 1.45	−0.94 ± 1.17	−2.77 ± 1.12	−0.33 ± 1.49	−0.26 ± 1.47	0.29 ± 1.17	−2.70 ± 1.15
Phe25	−1.99 ± 0.53	−2.27 ± 0.58	−2.92 ± 0.49	−1.69 ± 0.53	−1.16 ± 0.53	−1.47 ± 0.57	−1.82 ± 0.49	−1.27 ± 0.53
Lys29	0.17 ± 1.66	0.10 ± 2.01	0.53 ± 1.54	0.12 ± 1.84	0.31 ± 1.64	0.75 ± 2.01	1.62 ± 1.51	−0.02 ± 1.82
Glu149	−6.15 ± 2.66	−4.09 ± 1.75	−1.71 ± 1.27	−6.20 ± 1.24	−6.62 ± 2.67	−4.68 ± 1.72	−2.33 ± 1.26	−6.84 ± 1.23
Ser150	−1.18 ± 0.66	−0.87 ± 0.78	−0.60 ± 0.62	−1.25 ± 0.62	0.77 ± 0.66	0.72 ± 0.77	0.69 ± 0.63	0.95 ± 0.62
Ser151	−1.09 ± 0.60	−0.86 ± 0.59	−0.80 ± 0.73	−1.09 ± 0.60	−0.94 ± 0.60	−0.76 ± 0.58	−0.68 ± 0.72	−0.92 ± 0.60
Pro152	−3.13 ± 0.43	−2.87 ± 0.49	−2.44 ± 0.45	−3.28 ± 0.43	−2.87 ± 0.43	−2.66 ± 0.49	−2.35 ± 0.44	−2.95 ± 0.43
Ser213	0.00 ± 0.69	−0.04 ± 0.63	−0.15 ± 0.74	−0.03 ± 0.65	0.51 ± 0.68	0.58 ± 0.62	1.44 ± 0.74	0.86 ± 0.63

Note: ± represents the standard errors of the mean.

Author contributions

R.A. acquired funding, conceived and directed the project, collated and analysed data, carried out molecular docking, ADMET studies; V.J. carried out molecular dynamics simulations and MM/PB(GB)SA calculations; C.B. carried out viral inhibition tests under supervision of P.A.; Manuscript was written by R.A. with contributions from V.J., C.B, P.A. and S.H.

Declaration of competing interest

Authors declare no conflict of interest.

Acknowledgement

Appendix A. Supplementary data

Supplementary data to this article can be found online at https://doi.org/10.1016/j.jtcme.2022.12.002.

References

1. Bhatt S, Gething PW, Brady OJ, et al. The global distribution and burden of dengue. *Nature*. 2013;496(7446):504–507. https://doi.org/10.1038/nature12060.
2. Wu Q, Dong S, Li X, et al. Effects of COVID-19 non-pharmacological interventions on dengue infection: a systematic review and meta-analysis. *Front Cell Infect Microbiol*. 2022;12. https://www.frontiersin.org/article/10.3389/fcimb.2022.892508. Accessed June 13, 2022.
3. Dighe SN, Ekwudu O, Dua K, Chellappan DK, Katavic PL, Collet TA. Recent update on anti-dengue drug discovery. *Eur J Med Chem*. 2019;176:431–455. https://doi.org/10.1016/j.ejmech.2019.05.010.
4. Lim SP. Dengue drug discovery: progress, challenges and outlook. *Antivir Res*. 2019;163:156–178. https://doi.org/10.1016/j.antiviral.2018.12.016.
5. Lindenbach BD, Thiel HJ, Rice CM. *Fields Virology Chapter 33; Flaviviridae: The Viruses and Their Replication*. fifth ed. Lippincott-Raven Publishers; 2007.
6. Dong H, Fink K, Züst R, Lim SP, Qin CF, Shi PY. Flavivirus RNA methylation. *J Gen Virol*. 2014;95(4):763–778. https://doi.org/10.1099/vir.0.062208-0.
7. Egloff MP, Benarroch D, Selisko B, Romette JL, Canard B. An RNA cap (nucleoside-2′-O-)-methyltransferase in the flavivirus RNA polymerase NS5: crystal structure and functional characterization. *EMBO J*. 2002;21(11):2757–2768. https://doi.org/10.1093/emboj/21.11.2757.
8. Brecher M, Chen H, Li Z, et al. Identification and characterization of novel broad-spectrum inhibitors of the flavivirus methyltransferase. *ACS Infect Dis*. 2015;1(8):340–349. https://doi.org/10.1021/acsinfecdis.5b00070.
9. Lim SP, Sonntag LS, Noble C, et al. Small molecule inhibitors that selectively block dengue virus methyltransferase. *J Biol Chem*. 2011;286(8):6233–6240. https://doi.org/10.1074/jbc.M110.179184.
10. W P, Eaf M. Update on methyltransferase inhibitors of the dengue virus and further scope in the field. *J Emerg Infect Dis*. 2016;1(2). https://doi.org/10.4172/2472-4998.1000108.
11. Benmansour F, Trist I, Coutard B, et al. Discovery of novel dengue virus NS5 methyltransferase non-nucleoside inhibitors by fragment-based drug design. *Eur J Med Chem*. 2017;125:865–880. https://doi.org/10.1016/j.ejmech.2016.10.007.
12. Potenza MA, Montagnani M, Santacroce L, Charitos IA, Bottalico L. Ancient herbal therapy: a brief history of Panax ginseng. *J Ginseng Res*. 2022. https://doi.org/10.1016/j.jgr.2022.03.004. Published online March 23.
13. Yang Y, Ren C, Zhang Y, Wu X. Ginseng: an nonnegligible natural remedy for healthy aging. *Aging Dis*. 2017;8(6):708–720. https://doi.org/10.14336/AD.2017.0707.
14. Duan L, Xiong X, Hu J, Liu Y, Li J, Wang J. Panax notoginseng saponins for treating coronary artery disease: a functional and mechanistic overview. *Front Pharmacol*. 2017;8. https://www.frontiersin.org/article/10.3389/fphar.2017.00702. Accessed April 25, 2022.
15. Jeon WJ, Oh JS, Park MS, Ji GE. Anti-hyperglycemic effect of fermented ginseng in type 2 diabetes mellitus mouse model. *Phytother Res*. 2013;27(2):166–172. https://doi.org/10.1002/ptr.4706.
16. Ng TB. Pharmacological activity of sanchi ginseng (*Panax notoginseng*). *J Pharm Pharmacol*. 2010;58(8):1007–1019. https://doi.org/10.1211/jpp.58.8.0001.
17. Ratan ZA, Rabbi Mashrur F, Runa NJ, Kwon KW, Hosseinzadeh H, Cho JY. Ginseng, a promising choice for SARS-COV-2: a mini review. *J Ginseng Res*. 2022;46(2):183–187. https://doi.org/10.1016/j.jgr.2022.01.004.
18. Ali SI, Sheikh WM, Rather MA, Venkatesalu V, Muzamil Bashir S, Nabi SU. Medicinal plants: treasure for antiviral drug discovery. *Phytother Res*. 2021. https://doi.org/10.1002/ptr.7039. Published online February 16.
19. Zhang F, He J, Peng J, et al. Guidelines for the diagnosis and treatment of dengue in China. *Infect Dis Immun*. 2021;1(3):144–152. https://doi.org/10.1097/ID9.0000000000000026.
20. Zheng Y ru, C lin Fan, Chen Y, et al. Anti-inflammatory, anti-angiogenetic and antiviral activities of dammarane-type triterpenoid saponins from the roots of Panax notoginseng. *Food Funct*. 2022;13(6):3590–3602. https://doi.org/10.1039/D1FO04089H.
21. Lim SYM, Chieng JY, Pan Y. Recent insights on anti-dengue virus (DENV) medicinal plants: review on in vitro, in vivo and in silico discoveries. *Life*. 2021;14(1):1–33. https://doi.org/10.1080/26895293.2020.1856192.
22. Sliwoski G, Kothiwale S, Meiler J, Lowe EW. Computational methods in drug discovery. *Pharmacol Rev*. 2014;66(1):334–395. https://doi.org/10.1124/pr.112.007336.
23. Pagadala NS, Syed K, Tuszynski J. Software for molecular docking: a review. *Biophys Rev*. 2017;9(2):91–102. https://doi.org/10.1007/s12551-016-0247-1.
24. Lyu J, Wang S, Balius TE, et al. Ultra-large library docking for discovering new chemotypes. *Nature*. 2019;566(7743):224–229. https://doi.org/10.1038/s41586-019-0917-9.
25. Lionta E, Spyrou G, Vassilatis DK, Cournia Z. Structure-based virtual screening for drug discovery: principles, applications and recent advances. *Curr Top Med Chem*. 2014;14(16):1923–1938. https://doi.org/10.2174/1568026614666140929124445.
26. Bhakat S, Delang L, Kaptein S, Neyts J, Leyssen P, Jayaprakash V. Reaching beyond HIV/HCV: nelfinavir as a potential starting point for broad-spectrum protease inhibitors against dengue and chikungunya virus. *RSC Adv*. 2015;5(104):85938–85949. https://doi.org/10.1039/C5RA14469H.
27. Yi D, Li Q, Pang L, et al. Identification of a broad-spectrum viral inhibitor targeting a novel allosteric site in the RNA-dependent RNA polymerases of dengue virus and norovirus. *Front Microbiol*. 2020;11. https://doi.org/10.3389/fmicb.2020.01440.
28. Singh R, Bhardwaj VK, Sharma J, Purohit R, Kumar S. In-silico evaluation of bioactive compounds from tea as potential SARS-CoV-2 nonstructural protein 16 inhibitors. *J Tradit Complement Med*. 2021;12(4):335–344. https://doi.org/10.1016/j.jtcme.2021.05.005.
29. Durrant JD, McCammon JA. Molecular dynamics simulations and drug discovery. *BMC Biol*. 2011;9(1):71. https://doi.org/10.1186/1741-7007-9-71.
30. Trott O, Olson AJ. AutoDock Vina: improving the speed and accuracy of docking with a new scoring function, efficient optimization, and multithreading. *J Comput Chem. Published online*. 2009:455–461. https://doi.org/10.1002/jcc.21334.
31. Home | computational insights into drug discovery. http://www.lephar.com/index.htm. Accessed June 9, 2022.
32. The PyMOL Molecular Graphics System, Version 1.5 Schrödinger, LLC.
33. Open Babel. http://openbabel.org/wiki/Main_Page. Accessed April 17, 2022.
34. O'Boyle NM, Banck M, James CA, Morley C, Vandermeersch T, Hutchison GR. Open Babel: an open chemical toolbox. *J Cheminf*. 2011;3(1):33. https://doi.org/10.1186/1758-2946-3-33.
35. Meeko: preparation of small molecules for AutoDock. Published online June 6 https://github.com/forlilab/Meeko; 2022. Accessed June 10, 2022.
36. *Schrödinger Release 2021-3*. New York, NY: Maestro, Schrödinger, LLC; 2021.
37. Daina A, Michielin O, Zoete V. SwissADME: a free web tool to evaluate pharmacokinetics, drug-likeness and medicinal chemistry friendliness of small molecules. *Sci Rep*. 2017;7(1), 42717. https://doi.org/10.1038/srep42717.
38. Abraham MJ, Murtola T, Schulz R, et al. GROMACS: high performance molecular simulations through multi-level parallelism from laptops to supercomputers. *Software*. 2015;1–2:19–25. https://doi.org/10.1016/j.softx.2015.06.001.
39. Maier JA, Martinez C, Kasavajhala K, Wickstrom L, Hauser KE, Simmerling C. ff14SB: improving the accuracy of protein side chain and backbone parameters from ff99SB. *J Chem Theor Comput*. 2015;11(8):3696–3713. https://doi.org/10.1021/acs.jctc.5b00255.
40. Wang J, Wolf RM, Caldwell JW, Kollman PA, Case DA. Development and testing of a general amber force field. *J Comput Chem*. 2004;25(9):1157–1174. https://doi.org/10.1002/jcc.20035.
41. Jorgensen WL, Chandrasekhar J, Madura JD, Impey RW, Klein ML. Comparison of simple potential functions for simulating liquid water. *J Chem Phys*. 1983;79(2):926–935. https://doi.org/10.1063/1.445869.
42. Case DA, Aktulga HM, Belfon K, et al. *Amber 2021*. San Francisco: University of California; 2021.
43. Shirts MR, Klein C, Swails JM, et al. Lessons learned from comparing molecular dynamics engines on the SAMPL5 dataset. *J Comput Aided Mol Des*. 2017;31(1):147–161. https://doi.org/10.1007/s10822-016-9977-1.
44. Frisch MJ, Trucks GW, Schlegel HB, et al. Gaussian 16 Rev. C.01. Published online 2016.
45. Bayly CI, Cieplak P, Cornell W, Kollman PA. A well-behaved electrostatic

potential based method using charge restraints for deriving atomic charges: the RESP model. *J Phys Chem*. 1993;97(40):10269–10280. https://doi.org/10.1021/j100142a004.

46. Bussi G, Donadio D, Parrinello M. Canonical sampling through velocity rescaling. *J Chem Phys*. 2007;126(1), 014101. https://doi.org/10.1063/1.2408420.

47. Parrinello M, Rahman A. Polymorphic transitions in single crystals: a new molecular dynamics method. *J Appl Phys*. 1981;52(12):7182–7190. https://doi.org/10.1063/1.328693.

48. Hess B, Bekker H, Berendsen HJC, Fraaije JGEM. LINCS: a linear constraint solver for molecular simulations. *J Comput Chem*. 1997;18(12):1463–1472. https://doi.org/10.1002/(SICI)1096-987X(199709)18:12<1463::AID-JCC4>3.0.CO;2-H.

49. Darden T, York D, Pedersen L. Particle mesh Ewald: an N·log(N) method for Ewald sums in large systems. *J Chem Phys*. 1993;98(12):10089–10092. https://doi.org/10.1063/1.464397.

50. Miller BR, McGee TD, Swails JM, Homeyer N, Gohlke H, Roitberg AE. MMPBSA.py: an efficient Program for end-state free energy calculations. *J Chem Theor Comput*. 2012;8(9):3314–3321. https://doi.org/10.1021/ct300418h.

51. Valdés-Tresanco MS, Valdés-Tresanco ME, Valiente PA, gmx_Mmpbsa Moreno E. A new tool to perform end-state free energy calculations with GROMACS. *J Chem Theor Comput*. 2021;17(10):6281–6291. https://doi.org/10.1021/acs.jctc.1c00645.

52. Humphrey W, Dalke A, Schulten K. VMD: visual molecular dynamics. *J Mol Graph*. 1996;14(1):33–38. https://doi.org/10.1016/0263-7855(96)00018-5.

53. Lai YL, Chung YK, Tan HC, et al. Cost-effective real-time reverse transcriptase PCR (RT-PCR) to screen for dengue virus followed by rapid single-tube multiplex RT-PCR for serotyping of the virus. *J Clin Microbiol*. 2007;45(3):935–941. https://doi.org/10.1128/JCM.01258-06.

54. Nishimori H, Shiratsuchi T, Urano T, et al. A novel brain-specific p53-target gene, Bai1, containing thrombospondin type 1 repeats inhibits experimental angiogenesis. *Oncogene*. 1997;15(18):2145–2150. https://doi.org/10.1038/sj.onc.1201542.

55. Home - GraphPad. https://www.graphpad.com/. Accessed November 21, 2022.

56. Noble CG, Li SH, Dong H, Chew SH, Shi PY. Crystal structure of dengue virus methyltransferase without S-adenosyl-L-methionine. *Antivir Res*. 2014;111:78–81. https://doi.org/10.1016/j.antiviral.2014.09.003.

57. Benarroch D, Egloff MP, Mulard L, Guerreiro C, Romette JL, Canard B. A structural basis for the inhibition of the NS5 dengue virus mRNA 2′-O-methyltransferase domain by Ribavirin 5′-triphosphate. *J Biol Chem*. 2004;279(34):35638–35643. https://doi.org/10.1074/jbc.M400460200.

58. Mysinger MM, Carchia M, Irwin JohnJ, Shoichet BK. Directory of useful decoys, enhanced (DUD-E): better ligands and decoys for better benchmarking. *J Med Chem*. 2012;55(14):6582–6594. https://doi.org/10.1021/jm300687e.

59. Liu H, Lu X, Hu Y, Fan X. Chemical constituents of Panax ginseng and Panax notoginseng explain why they differ in therapeutic efficacy. *Pharmacol Res*. 2020;161, 105263. https://doi.org/10.1016/j.phrs.2020.105263.

60. Oh KK, Adnan Md, Cho DH. The promising mechanisms of low molecular weight compounds of Panax ginseng C.A. Meyer in alleviating COVID-19: a network pharmacology analysis. *Processes*. 2022;10(2):333. https://doi.org/10.3390/pr10020333.

61. Park SY, Park JH, Kim HS, et al. Systems-level mechanisms of action of Panax ginseng: a network pharmacological approach. *J Ginseng Res*. 2018;42(1):98–106. https://doi.org/10.1016/j.jgr.2017.09.001.

62. Jeffrey GA. *An Introduction to Hydrogen Bonding*. Oxford University Press; 1997.

63. Manjula S, Kumaradhas P. Evaluating the suitability of RNA intervention mechanism exerted by some flavonoid molecules against dengue virus MTase RNA capping site: a molecular docking, molecular dynamics simulation, and binding free energy study. *J Biomol Struct Dyn*. 2020;38(12):3533–3543. https://doi.org/10.1080/07391102.2019.1666744.

64. Zhao Y, Soh TS, Lim SP, et al. Molecular basis for specific viral RNA recognition and 2′-O-ribose methylation by the dengue virus nonstructural protein 5 (NS5). *Proc Natl Acad Sci USA*. 2015;112(48):14834–14839. https://doi.org/10.1073/pnas.1514978112.

65. Dong H, Chang DC, Xie X, et al. Biochemical and genetic characterization of dengue virus methyltransferase. *Virology*. 2010;405(2):568–578. https://doi.org/10.1016/j.virol.2010.06.039.

66. Coulerie P, Maciuk A, Eydoux C, et al. New inhibitors of the DENV-NS5 RdRp from carpolepis laurifolia as potential antiviral drugs for dengue treatment. *Rec Nat Prod. Published online*. 2014:4.

67. PubChem. Isoquercitrin. Accessed May 23, 2022. https://pubchem.ncbi.nlm.nih.gov/compound/5280804.

68. Evaluating the bioavailability of isoquercetin. https://www.naturalmedicinejournal.com/journal/evaluating-bioavailability-isoquercetin. Accessed May 23, 2022.

69. Weignerová L, Marhol P, Gerstorferová D, Křen V. Preparatory production of quercetin-3-β-d-glucopyranoside using alkali-tolerant thermostable α-l-rhamnosidase from Aspergillus terreus. *Bioresour Technol*. 2012;115:222–227. https://doi.org/10.1016/j.biortech.2011.08.029.

70. Mbikay M, Chrétien M. Isoquercetin as an anti-covid-19 medication: a potential to realize. *Front Pharmacol*. 2022;13, 830205. https://doi.org/10.3389/fphar.2022.830205.

71. de Sousa LRF, Wu H, Nebo L, et al. Flavonoids as noncompetitive inhibitors of Dengue virus NS2B-NS3 protease: inhibition kinetics and docking studies. *Bioorg Med Chem*. 2015;23(3):466–470. https://doi.org/10.1016/j.bmc.2014.12.015.

72. Valentová K, Vrba J, Bancířová M, Ulrichová J, Křen V. Isoquercitrin: pharmacology, toxicology, and metabolism. *Food Chem Toxicol*. 2014;68:267–282. https://doi.org/10.1016/j.fct.2014.03.018.

73. Khan H, Belwal T, Efferth T, et al. Targeting epigenetics in cancer: therapeutic potential of flavonoids. *Crit Rev Food Sci Nutr*. 2021;61(10):1616–1639. https://doi.org/10.1080/10408398.2020.1763910.

74. Zwicker JI, Schlechter BL, Stopa JD, et al. Targeting protein disulfide isomerase with the flavonoid isoquercetin to improve hypercoagulability in advanced cancer. JCI Insight. 4(4):e125851. doi:10.1172/jci.insight.125851.

75. Magar RT, Sohng JK. A review on structure, modifications and structure-activity relation of quercetin and its derivatives. *J Microbiol Biotechnol*. 2020;30(1):11–20. https://doi.org/10.4014/jmb.1907.07003.